Submicroscopic exsolution in Mn-bearing alkali amphiboles from Tirodi, Maharashtra, India

YEN-HONG SHAU*, DONALD R. PEACOR

Department of Geological Sciences, University of Michigan, Ann Arbor, Michigan 48109, U.S.A.

SUBRATA GHOSE

Department of Geological Sciences, University of Washington, Seattle, Washington 98195, U.S.A.

P. P. PHAKEY

Department of Physics, Monash University, Clayton, Victoria 3168, Australia

ABSTRACT

Submicroscopic exsolution in Mn-bearing alkali amphibole from Tirodi, Maharashtra, India, has been studied with transmission and analytical electron microscopy (TEM and AEM). The amphibole (crystals up to a few centimeters long) exhibits submicroscopic exsolution textures and has an average bulk composition $(K_{0.11}Na_{0.55})(Na_{0.93}-Ca_{0.41}Mn_{0.66})(Mn_{0.05}Fe^{2+}_{0.52}Mg_{4.08}Fe^{3+}_{0.29}Ti_{0.01}Al_{0.05})(Si_{7.90}Al_{0.10})O_{22}(OH)_2$, that is intermediate to magnesio-arfvedsonite, magnesio-riebeckite, manganese-cummingtonite, and richterite. The amphibole contains sparse inclusions (a few micrometers wide) of two secondary amphiboles, magnesio-arfvedsonite with a magnesio-riebeckite component, $(K_{0.18}Na_{0.44})-(Na_{1.96}Ca_{0.03}Mn_{0.01})(Mn_{0.08}Fe^{2+}_{0.79}Mg_{2.83}Fe^{3+}_{1.13}Ti_{0.06}Al_{0.11})(Si_{7.99}Al_{0.01})O_{22}(OH)_2$, and manganese-cummingtonite with a richterite component, $(K_{0.01}Na_{0.62})(Na_{0.28}Ca_{0.29}Mn_{1.43})-(Mn_{0.47}Fe^{2+}_{0.01}Mg_{4.52})(Si_{7.88}Al_{0.03})O_{22}(OH)_2$, which do not exhibit exsolution textures.

Two sets of exsolution lamellae were observed in the coarse amphibole crystals: "$\bar{1}01$" lamellae oriented ~11° from $(\bar{1}01)$, and "100" lamellae oriented ~4.5° from (100). The orientations of these exsolution lamellae are consistent with predicted orientations, on the basis of optimal phase boundary theory. The (110) lattice fringes are continuous across interfaces of the "$\bar{1}01$" lamellae but change orientation by about 1.5° when viewed parallel to $[1\bar{1}2]$, implying coherent interfaces with minimum strain. The AEM analyses of both sets of lamellae and hosts give paired compositions that approach those of the two secondary amphiboles with no exsolution. The microstructures are consistent with an origin through spinodal decomposition, although homogeneous nucleation and growth is not completely excluded for the "$\bar{1}01$" and some of the "100" lamellae.

The exsolution texture in the primary Mn-bearing alkali amphibole and the presence of coexisting secondary amphiboles are consistent with a miscibility gap between alkali amphibole and ferromagnesian amphibole. Major differences in M4 site occupancies (Na vs. Mn) coupled with differences in M2 site occupancies (Fe^{3+} vs. Mg) imply that the exsolution relations are primarily controlled by occupancies of the M4 and M2 sites and can be ideally expressed by the substitution $^{[M4]}Na^+ + {}^{[M2]}Fe^{3+} \leftrightarrow {}^{[M4]}Mn^{2+} + {}^{[M2]}Mg^{2+}$. The two types of associated amphibole inclusions with compositions close to magnesio-arfvedsonite and manganese-cummingtonite with some richterite component, respectively, are inferred to have formed by dissolution-crystallization during retrograde metamorphism or subsequent hydrothermal alteration.

INTRODUCTION

Amphiboles, a group of silicate minerals exhibiting wide ranges of solid solution, may coexist as two or more separate phases or as exsolution-derived intergrowths, commonly resulting from the existence of solvi between am-
phibole subgroups (ferromagnesian, calcic, sodic-calcic, and alkali amphiboles; Leake, 1978) or within a subgroup (e.g., ferromagnesian orthoamphiboles and calcic amphiboles) in metamorphic rocks (e.g., Ghose, 1981; Robinson et al., 1982; Smelik et al., 1991). There have been many reports of two or more (up to five) coexisting amphiboles (e.g., Ghose, 1981; Robinson et al., 1982; Spear, 1982; Kimball and Spear, 1984; Evans, 1986; Smelik and Veblen, 1989, 1991; Smelik et al., 1991). The presence

* Current address: Department of Marine Resources, National Sun Yat-sen University, Kaohsiung 804, Taiwan, Republic of China.

of miscibility gaps and their extent among amphiboles have been shown to be largely related to the radii and charge of the cations that occupy the A, M4, M2, and T sites. For example, the actinolite-hornblende miscibility gap involves cations in the A, M2, and T sites (e.g., Smelik et al., 1991), whereas that of glaucophane-cummingtonite primarily involves cations in the M4 and M2 sites (e.g., Smelik and Veblen, 1991).

Ghose et al. (1974) and Phakey and Ghose (1974) reported a miscibility gap between magnesio-richterite and magnesio-riebeckite based on a study of Mn-bearing alkali amphibole from Tirodi, Madhya Pradesh, India. Using single-crystal X-ray diffraction, electron microprobe (EMP) analyses, and transmission electron microscopy (TEM), they described two clinoamphiboles occurring as very fine-scale exsolution lamellae (~500 Å wide). However, the compositions obtained by EMP analyses were not definitive because of the overlap of the two phases by the electron beam, and the solvus relations among such Mn-rich alkali amphiboles remained ill-defined. We have therefore carried out a detailed study of these amphiboles using transmission and analytical electron microscopy (TEM and AEM), techniques that can resolve the structure and composition of the very fine-scale exsolution lamellae defined by Ghose et al. (1974). A brief summary of those results was given by Shau et al. (1989), and the detailed results are reported in this paper.

The name tirodite was first given by Dunn and Roy (1938) to straw yellow amphibole occurring as coarse-bladed prisms associated with braunite, spessartine, rhodonite, and quartz in a metamorphosed Mn formation at Tirodi, Maharashtra, India. The type material from Tirodi is essentially richterite in composition with significant amounts of Na in the A site and minor components of manganese-cummingtonite, magnesio-riebeckite, and magnesio-arfvedsonite. This amphibole is chemically distinct from manganoan cummingtonite or manganese-cummingtonite, $(Mg,Mn)_2Mg_5Si_8O_{22}(OH)_2$. Unfortunately, the name tirodite has been used as a general term for manganoan cummingtonite and accepted as the end-member $Mn_2Mg_5Si_8O_{22}(OH)_2$ (Leake, 1978). In a 1989 proposal to the IMA Commission on New Minerals and Mineral Names, Ghose and Peacor suggested that the name tirodite should be reserved as a varietal name for the complex alkali amphibole from the metamorphosed Mn formations. In this paper, we avoid using mineral names for both the Mn-bearing alkali amphibole and the Mn-rich end-member ferromagnesian amphibole. However, when necessary below, we have used the term "tirodite" (with quotation marks) to refer to the Mn-bearing alkali amphibole.

Mn-bearing alkali amphibole is common among the Mn-bearing amphiboles present in gondites of the Sausar group of Madhya Pradesh and Maharashtra, India. Gondites are regionally metamorphosed manganiferrous sedimentary rocks, characterized by spessartine and quartz with or without other manganese silicates, such as rhodonite and manganiferrous pyroxenes and amphiboles,

interbedded with other (pelitic and psammitic) sedimentary rocks. The Mn ore minerals (braunite, bixbyite, hollandite, hausmannite, jacobsite, etc.) associated with gondites are almost entirely of metamorphic origin (Roy, 1966). In gondites, Mn-bearing alkali amphibole occurs as fine straw yellow needles or blades associated with rhodonite, spessartine, and manganese oxides. Large prismatic crystals of Mn-bearing alkali amphibole (up to 25 cm in length, as in the Tirodi West Hill pegmatites) occur in Tirodi where pegmatites cut across gondites and Mn ore bodies. These occurrences are restricted to the sillimanite zone.

Samples of large crystals of the Mn-bearing alkali amphibole were collected by S.G. in 1980 from the Tirodi mine at Tirodi, Maharashtra. A number of the samples from Tirodi were also obtained from S. Roy, Jadavpur University, Calcutta.

ANALYTICAL TECHNIQUES AND NORMALIZATION OF AMPHIBOLE FORMULAE

Optical microscopy and scanning electron microscopy (SEM) were used in preliminary petrographic studies and mineral identification. A Hitachi S-570 SEM with a back-scattered electron (BSE) detector and energy-dispersive spectrometer (EDS) was utilized to examine polished thin sections and TEM specimens. Millimeter- to centimeter-sized crystals of the Mn-bearing alkali amphibole were used for preparing thin sections mounted with thermo-sensitive cement. The crystal grains were mounted in preferred orientations in which their **b** axes or **a*** axes were approximately perpendicular to the thin section surface. Specimens for TEM were then made from those thin sections by ion thinning selected areas (cf. Shau et al., 1990). A Philips CM-12 scanning transmission electron microscope (STEM) equipped with a Kevex Quantum detector (EDS system) was used for TEM and AEM analyses. Selected-area electron diffraction (SAED) patterns and multibeam images were obtained in the TEM mode, whereas AEM analyses were acquired in scanning mode, which allows for a small probe diameter of approximately 50 Å. By tilting the TEM specimens a few degrees, the **b** axis or **a** axis of amphibole crystals could be oriented parallel to the electron beam, giving [010] or [100] zone SAED patterns or images, respectively.

The CM-12 STEM was operated at 120 kV for both TEM and AEM analyses. Specimens were tilted toward the EDS detector by 20°, giving a take-off angle of 34° during AEM analysis. During analysis of very fine-scale exsolution lamellae, with the specimen tilted toward the detector, the lamellae interfaces were oriented parallel to the electron beam to minimize overlap in analyses of contiguous lamellae. Analyses of lamellae ≤500 Å wide were obtained using a point beam or a line scan along the lamellae. Bulk analyses including both unmixed phases were obtained by rastering the beam over square areas that were large enough to represent the average composition of the two phases (usually 4000 × 4000 Å² or larger). The X-ray spectra were acquired at 200–400 counts
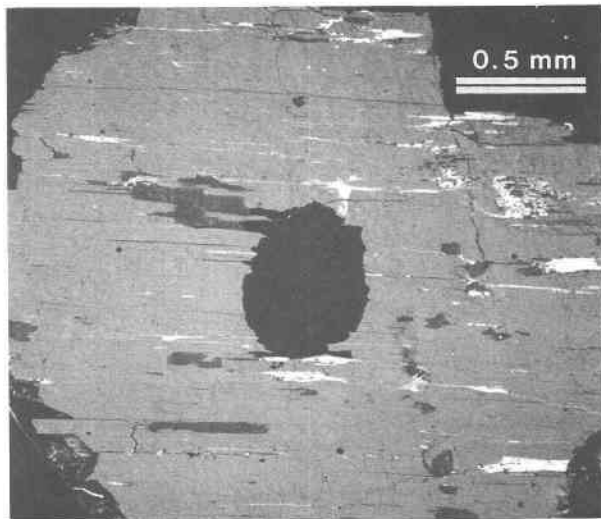
Fig. 1. A BSE image of a TEM thin-film specimen with thin edges (around the central black hole) created by Ar-beam ion thinning. The gray area is part of a large Mn-bearing alkali amphibole crystal that contains many elongated inclusions of quartz (dark gray), hollandite, pyrophanite, rutile, and manganese oxide (the last four minerals appear white).

per s for 200 s (live time). The thin foil approximation was adopted, using experimentally determined k factors for each element to derive quantitative results (Cliff and Lorimer, 1975). The precision of the AEM analyses, including errors from counting statistics and standardization processes, are comparable with those of conventional EMP analyses for major elements, although less precise for minor elements (cf. Shau et al., 1990, 1991).

A Cameca Camebax electron microprobe operated at 15 kV and a beam current of 10 nA was used to analyze amphiboles and other phases. The standards for EMP analyses include hornblende (Si, Al, Fe, Mg, Ca, Na), geikielite (Ti), rhodonite (Mn), potassium feldspar (K), fluorine topaz (F), and barium-chlorine apatite (Cl).

Structural formulae of amphiboles have been normalized according to criteria summarized by Robinson et al. (1982). The amphibole analyses were first normalized on the basis of 23 O, assuming all Fe^{2+}. If the resultant Si values were greater than 8, the formula was renormalized to 8 Si, and part of the Fe converted to Fe^{3+} (a resultant value that is a minimum estimate for the Fe^{3+} content) for charge balance. If a formula has Si $\leq$ 8 based on 23 O, the minimum Fe^{3+} content is 0. When there is a small amount of Al in the formula and Si + $Al_{tot} > 8$, normalization of Si + Al_{tot} to 8 gives a maximum estimated value for Fe^{3+}, assuming that no O substitutes for OH. However, if this normalization gave rise to unreasonable structural formulae (e.g., Na in M1 and M3 sites, or not enough Fe^{3+} for charge balance), the formulae would be recalculated with only part of the Al assigned to the tetrahedral site, and a smaller maximum Fe^{3+} value was then obtained to fulfill the crystal-chemical limit of am-
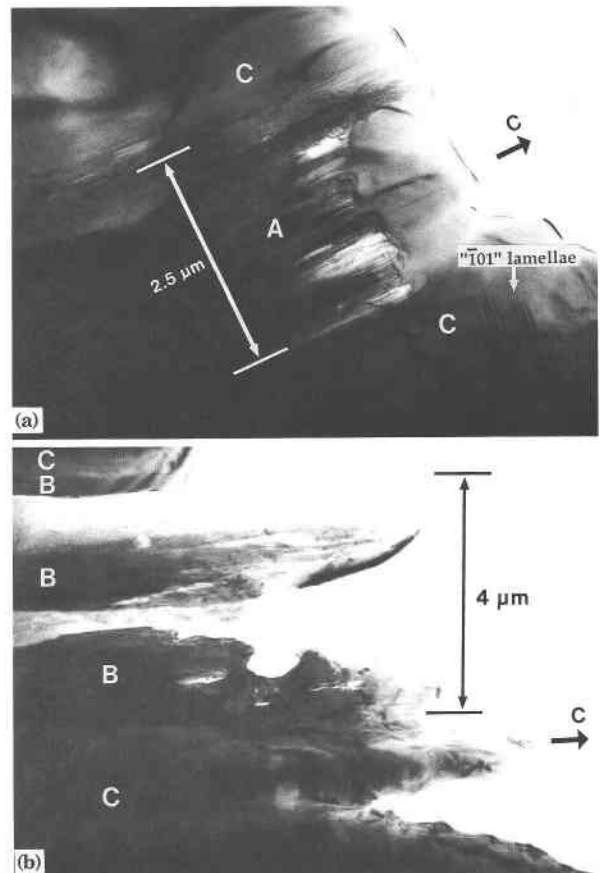

Fig. 2. Two [100] zone TEM multibeam bright field images showing the Mn-bearing alkali amphibole (C amphibole) and (a) the small A amphibole inclusions and (b) B amphibole inclusions. Abundant exsolved lamellae in the C amphibole have their projected traces nearly perpendicular to the c axis. The electron beam was approximately parallel to [100].

phiboles. The final estimated Fe^{3+} content was then derived from the average of the two ideal formulae containing minimum and maximum Fe^{3+} for each analysis. For AEM analyses, as the concentrations of elements (and oxides) for an analysis are all obtained relative to that of Si, weight percents of oxides presented here have been normalized assuming that oxides + calculated ideal H_2O = 100 wt%.

RESULTS

The Mn-bearing alkali amphibole crystals contain many inclusions of phases such as hollandite (also occurs as very thin veinlets), quartz, pyrophanite, rutile, and trace amounts of Mn oxide and hematite, as seen in BSE images (Fig. 1). An extremely fine (submicrometer) planar texture can barely be seen in one direction crosscutting the c axis in some amphibole crystals, when observed with the polarizing microscope.

Very small prismatic inclusions of amphiboles, which can only be identified by TEM, occur rarely within the

TABLE 1. Selected AEM and EMP analyses of Mn-bearing alkali amphiboles from Tirodi, Maharashtra, India

Oxides (wt%)	A		B	C*		C**	
	SKD	SR2*	SKD	SKD	SR2	SKD	SKD
SiO_2	56.37	55.76	55.36	55.84	55.81	55.49	55.47
Al_2O_3	0.96	0.71	0.18	0.78	0.90	0.56	0.59
TiO_2	0.00	0.56	0.00	0.28	0.09	0.03	0.31
Fe_2O_3†	7.44	10.48	0.00	1.60	2.72	5.64	5.17
FeO†	3.14	6.59	0.08	3.63	4.39	1.58	1.16
MgO	17.32	13.25	21.31	20.10	19.34	18.93	18.11
MnO	4.61	0.74	15.76	8.35	5.92	8.04	10.10
CaO	1.32	0.20	1.90	2.38	2.70	2.12	2.30
Na_2O	6.55	8.64	3.26	4.59	5.39	4.42	3.61
K_2O	0.17	0.98	0.05	0.33	0.61	0.11	0.28
F	n.d.	n.d.	n.d.	n.d.	n.d.	0.79	0.72
H_2O^+‡	2.12	2.09	2.10	2.12	2.12	1.71	1.74
−(O = F)	n.d.	n.d.	n.d.	n.d.	n.d.	−0.17	−0.15
TOTAL§	100.00	100.00	100.00	100.00	100.00	99.25	99.41
Si	7.95	7.99	7.88	7.90	7.90	7.97	7.98
[4]Al	0.05	0.01	0.03	0.10	0.10	0.03	0.02
TOTAL T site	8.00	8.00	7.91	8.00	8.00	8.00	8.00
[6]Al	0.11	0.11	0.00	0.03	0.05	0.07	0.08
Ti	0.00	0.06	0.00	0.03	0.01	0.00	0.03
Fe^{3+}	0.79	1.13	0.00	0.17	0.29	0.61	0.56
Mg	3.64	2.83	4.52	4.24	4.08	4.05	3.88
Fe^{2+}	0.37	0.79	0.01	0.43	0.52	0.19	0.14
Mn	0.09	0.08	0.47	0.10	0.05	0.08	0.31
TOTAL M1–M3	5.00	5.00	5.00	5.00	5.00	5.00	5.00
Mn	0.46	0.01	1.43	0.90	0.66	0.90	0.92
Ca	0.20	0.03	0.29	0.36	0.41	0.33	0.35
Na	1.34	1.96	0.28	0.74	0.93	0.77	0.73
TOTAL M4 site	2.00	2.00	2.00	2.00	2.00	2.00	2.00
Na	0.45	0.44	0.62	0.52	0.56	0.46	0.28
K	0.03	0.18	0.01	0.06	0.11	0.02	0.05
TOTAL A site	0.48	0.62	0.63	0.58	0.67	0.48	0.33
OH‡	2.00	2.00	2.00	2.00	2.00	1.64	1.67
F	n.d.	n.d.	n.d.	n.d.	n.d.	0.36	0.33

Note: Number of cations and Fe^{2+}/Fe^{3+} on the basis of normalization and charge balance; n.d. = not determined.
* Average of 3–4 analyses.
** Analyzed with the electron microprobe.
† Calculated based on normalized structural formulae.
‡ Calculated assuming 2(OH,F) per structural formula.
§ Assuming oxides + H_2O^+ = 100 wt% for AEM analyses.

principal crystal of the Mn-bearing alkali amphibole. It was difficult to distinguish such included amphiboles by optical microscopy and BSE imaging because of their fine size and because they have BSE image contrast similar to that of the porphyroblasts. However, when observed by TEM, they were seen to occur as prisms elongated parallel to the c axis and only a few micrometers wide (Fig. 2). They have sharp and straight boundaries parallel to the c axis and sharp boundaries terminating the ends of the prisms (Fig. 2a). Interestingly, these amphibole inclusions do not contain exsolution lamellae, although the surrounding amphibole porphyroblast invariably exhibits lamellar textures.

On the basis of AEM analyses, there are two kinds of amphibole inclusions whose compositions differ significantly with respect to amounts of Fe, Mn, Na, and Mg (Table 1). One phase with high contents of Fe and Na was designated as A amphibole, whereas the other phase, which is nearly free of Fe and has high Mn and Mg contents, was designated as B amphibole. The dominant amphibole, designated as C amphibole and containing abundant exsolution lamellae, has a bulk composition falling approximately between the compositions of the A and B

amphiboles (Table 1). Data from TEM images and SAED patterns indicate that both A and B amphiboles have the same crystallographic orientation as the C amphibole. All three amphiboles are thus intergrown topotaxially. Both A and B amphiboles were observed in sample SKD. The compositions of "$\bar{1}01$" and "100" lamellae occurring within the C amphibole were only obtained from sample SR2; the B phase was not observed in this sample, probably by chance, because it occurs only rarely. Chain-width variations producing slabs of wide-chain material [occurring parallel to (010)] were observed in some of the A and B amphiboles. These defects were not observed in the C amphibole.

The composition of the C amphibole from sample SKD was also obtained with EMP analysis (Table 1). The compositions obtained with EMP analysis are in very good agreement with the data obtained by AEM analysis, except that the calculated Fe^{3+}/Fe^{2+} ratios based on structural formula and charge balance are generally higher for the EMP analyses. The C amphibole contains 0.23–1.07 wt% of F and neglible Cl (0.00–0.02 wt%).

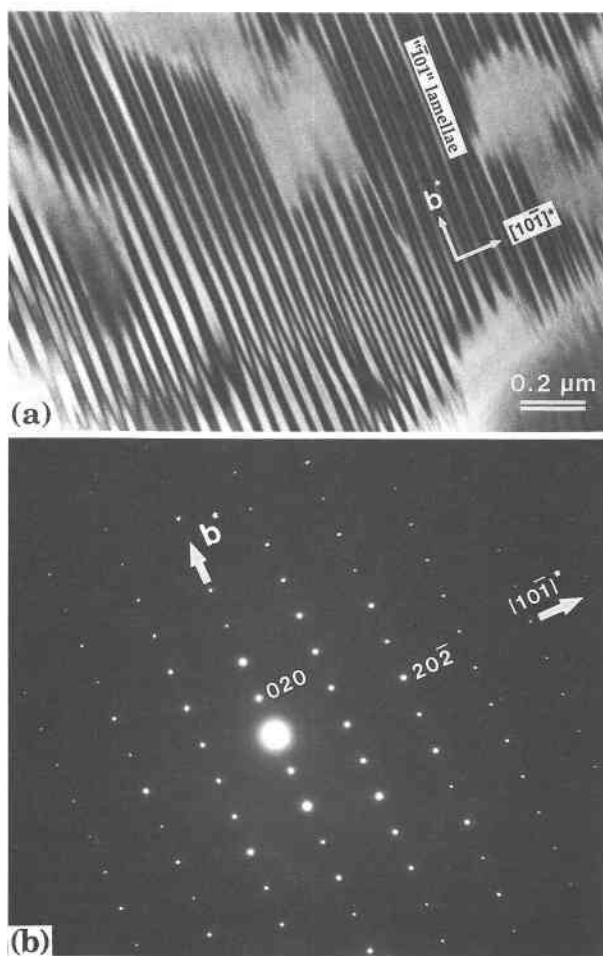Figure 3a is a [101] zone TEM bright field image of the dominant C amphibole showing "$\bar{1}01$" lamellae [irra-

Fig. 3. (a) A [101] zone TEM multibeam bright field image of "$\bar{1}$01" lamellae. The boundaries between the lamellae are not well defined, although the contrast is sharp, because of the inclination of the lamellar interface to the beam. Patches without clearly defined lamellae are of unknown origin. (b) Corresponding SAED pattern showing that the magnitudes of $\mathbf{b}^*$ and [10$\bar{1}$]* of the unmixed phases are nearly identical.

tional planes that are almost parallel to ($\bar{1}$01), cf. Robinson et al., 1971] about 300 Å in thickness. The traces of the "$\bar{1}$01" lamellae are parallel to the $\mathbf{b}$ axis, but the images of the interfaces between lamellae are not sharp because the "$\bar{1}$01" lamellae are inclined to the electron beam by ~12°, although ($\bar{1}$01) is parallel to the beam. The "100" lamellae cannot be readily observed because the (100) planes are oriented nearly perpendicular to the beam direction (~72°). The SAED patterns obtained for this orientation show only a single set of reflections, indicating that the magnitudes of the $\mathbf{b}$ axis and [10$\bar{1}$]* of the two exsolved phases are nearly identical (Fig. 3b). There are patches that exhibit vaguely defined lamellae that occur within areas with well-defined lamellae. No differences in composition could be detected between such patches and surrounding amphibole, and no variation in

their appearance was detected with varying exposure to the beam, implying that they are not caused by beam damage. We speculate that they may be a strain feature but cannot offer a definitive explanation.

In another orientation, with [010] nearly parallel to the beam, both sets of exsolution lamellae, "$\bar{1}$01" and "100", can be seen in the TEM images (Fig. 4a). The "$\bar{1}$01" lamellae are 100–150 Å thick, with the host lamellae being 200–300 Å thick, and have well-defined boundaries, whereas the "100" lamellae are only approximately 50 Å wide and exhibit wavy and ill-defined boundaries. The SAED patterns show reflections characteristic of both sets of lamellae (Fig. 4b). The "$\bar{1}$01" lamellae and host contribute two sets of reflections, which occur in slightly split pairs. Diffuse streaks connect the members of any pair and are oriented perpendicular to the "$\bar{1}$01" lamellae in real space. The diffuse streaks deviate by approximately 11° from [10$\bar{1}$]*, showing that the interfaces of "$\bar{1}$01" lamallae deviate from ($\bar{1}$01) by ~11° (Fig. 4b). The "100" lamellae give rise only to diffuse streaks, which are perpendicular to the "100" lamellae. There is ~4.5° deviation of the "100" lamellar interface from (100). Figure 5 is an image showing "$\bar{1}$01" lamallae 200–300 Å thick with well-defined boundaries and very fine-scale "100" lamellae with ill-defined boundaries. The A amphibole on the right side of Figure 5 does not exhibit any exsolution texture.

The AEM analyses can resolve and discriminate between the compositions of the "$\bar{1}$01" lamellae, as shown by the data of Table 2. The normalized structural formulae show that the narrower lamellae ~200 Å wide are enriched in Mg and Mn, whereas the thicker host lamellae (500–1000 Å thick) are enriched in Fe^{3+} and Na (Fig. 5). Analyses for the "100" lamellae and host were obtained within the "$\bar{1}$01" host. The "100" lamellae show similar trends in composition toward the A and B amphiboles, respectively, but to a much smaller extent, with the analyses of the individual lamellae being much closer to the average of the two. This is because the "100" lamellae are extremely narrow and at the limit of resolution for the AEM technique. Therefore, there must have been some lack of resolution of individual lamellae during analysis, and the analyses do not represent the true one-phase compositions.

Figure 6 is a [1$\bar{1}$2] zone TEM multibeam bright field image obtained by using the central beam and 110 reflections. The (110) lattice fringes are continuous across the "$\bar{1}$01" lamellar interfaces but show a slight lattice rotation of approximately 1.5°.

Although "$\bar{1}$01" lamellae are usually thicker than "100" lamellae, some amphibole grains have "$\bar{1}$01" and "100" lamellae that have similar thicknesses (~300 Å, Fig. 7). Such textures give rise to cross-shaped reflections that consist of two pairs of split reflections, each pair connected by a diffuse streak and caused by one set of lamellae.

The SAED patterns of all amphiboles of the present study are consistent with those of clinoamphiboles with space group $C2/m$. The lattice parameters of each of the
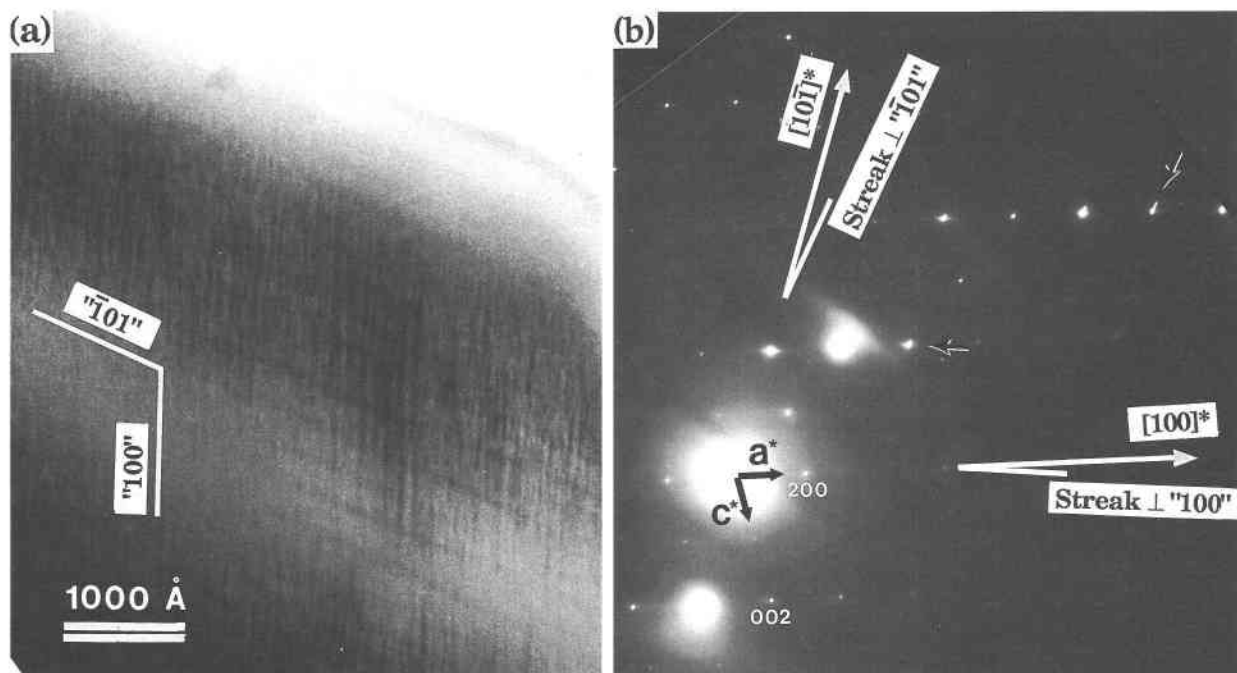
Fig. 4. (a) A TEM multibeam bright field image showing "$\bar{1}01$" lamellae and thinner "100" lamellae in the Mn-bearing alkali amphibole. The "$\bar{1}01$" lamellae are viewed parallel to the interface, but the "100" lamellae are slightly inclined to the beam. (b) Corresponding SAED pattern showing additional sets of reflections and streaks contributed by the "$\bar{1}01$" lamellae, and weak streaks from the "100" lamellae (both types of streaks are indicated by black arrows). The [010] zone axis is slightly inclined to the beam and toward the lower right, with the tilt axis perpendicular to the "$\bar{1}01$" lamellae.

two sets of "$\bar{1}01$" lamellae were determined from the SAED patterns. As there was no internal calibration of SAED patterns, only the differences in parameters of parallel lamellae are accurate (Table 3). The major differences in lattice parameters are between the values of a and β, which are slightly larger for the Na-Fe^{3+}-rich phase (the host in Figs. 4, 5) than for the Mn-Mg-rich phase (the "$\bar{1}01$" lamellae). The lattice parameters for these two phases are similar to those of magnesio-arfvedsonite and manganese-cummingtonite, respectively (Robinson et al., 1971).

TABLE 2. Selected AEM analyses of "$\bar{1}01$" and "100" lamellae, and hosts in the C amphibole

	"$\bar{1}01$"A host	"$\bar{1}01$"B lamella	"100"A host	"100"B lamella
Si	7.96	7.92	7.97	7.95
[4]Al	0.04	0.08	0.03	0.05
TOTAL T site	8.00	8.00	8.00	8.00
[6]Al	0.06	0.03	0.10	0.09
Ti	0.03	0.00	0.00	0.01
Fe^{3+}	0.64	0.13	0.84	0.51
Mg	3.86	4.26	3.62	3.97
Fe^{2+}	0.20	0.58	0.23	0.32
Mn	0.21	0.00	0.21	0.10
TOTAL M1–M3	5.00	5.00	5.00	5.00
Fe^{2+}	0.00	0.04	0.00	0.00
Mn	0.42	0.89	0.43	0.49
Ca	0.47	0.38	0.31	0.40
Na	1.11	0.69	1.26	1.11
TOTAL M4 site	2.00	2.00	2.00	2.00
Na	0.27	0.53	0.29	0.45
K	0.12	0.09	0.07	0.10
TOTAL A site	0.39	0.62	0.36	0.55

Fig. 5. A [010] zone TEM multibeam bright field image showing the "$\bar{1}01$" lamellae and vague "100" lamellae in the C amphibole and a lack of lamellae in the A amphibole.

Note: Number of cations and Fe^{2+}/Fe^{3+} on the basis of normalization and charge balance. Each analysis is an average of 2–3 point analyses. Subscripts A and B indicate that the analyzed phases have compositions close to those of A and B amphiboles, respectively.
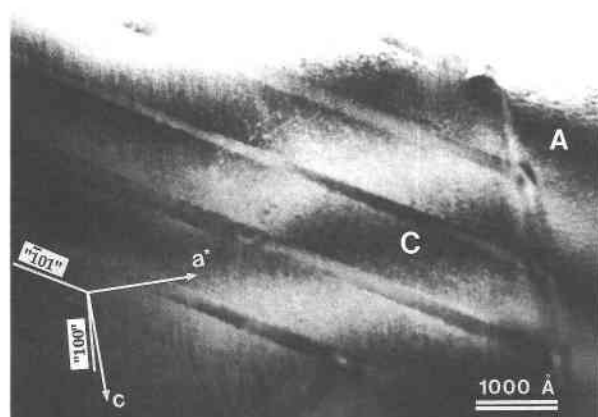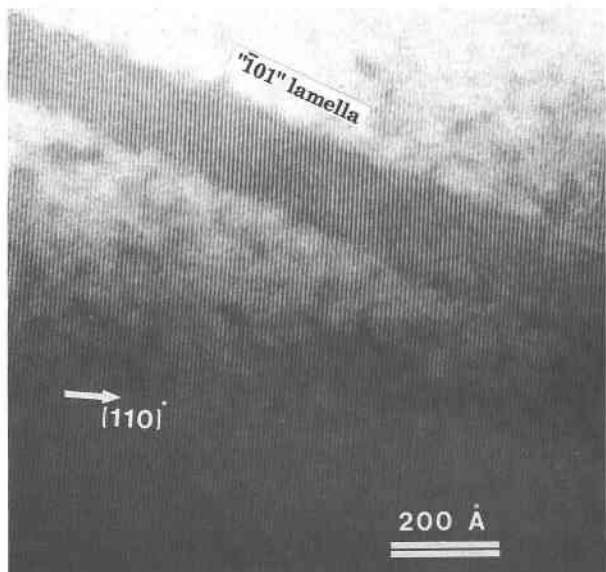
Fig. 6. A [$1\bar{1}2$] zone high-resolution TEM image showing (110) lattice fringes that are continuous across the lamellar boundary, but with a slight rotation of ~1.5° (best viewed by looking along the fringes, with the direction of view nearly parallel to the page).

DISCUSSION

Miscibility gap between alkali amphibole and ferromagnesian amphibole

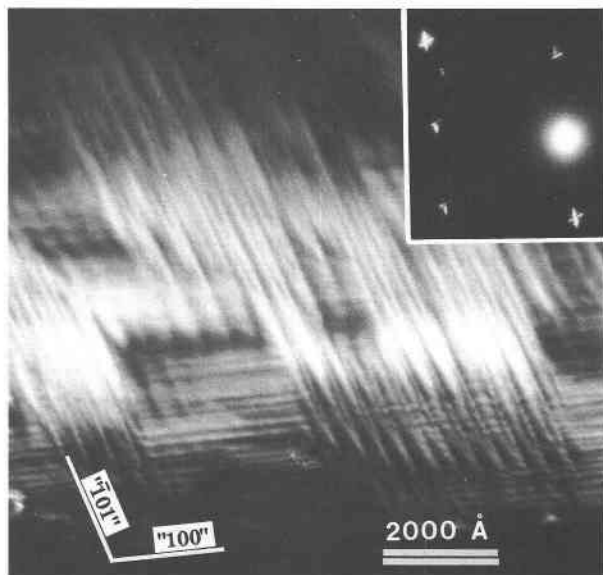The coexisting Mn-bearing alkali amphiboles from Tirodi include the dominant C amphibole and rare A and

Fig. 7. A TEM dark field image showing two sets of exsolved lamellae in approximately the same proportions and with similar widths. Inserted SAED pattern showing cross-shaped reflections. Diffuse streaks are superimposed on two pairs of split reflections, each pair derived from lamellae of different orientation.

TABLE 3. Lattice parameters and orientation relationships of "$\bar{1}01$" and "100" exsolution lamellae in the C amphibole

	"$\bar{1}01$"$_A$, host Na-Fe^{3+}-rich	"$\bar{1}01$"$_B$, lamellae Mn-Mg-rich
a	9.75(10) Å	9.62(10) Å
b	18.10(18) Å	18.10(18) Å
c	5.31(5) Å	5.31(5) Å
β	103.5(1)°	102.0(1)°
	"$\bar{1}01$" ∧ ($\bar{1}01$) = 11.3(5)°	
	"100" ∧ (100) = 4.5(5)°	
	"$\bar{1}01$" ∧ "100" = 114.7(5)°	
	($\bar{1}01$) ∧ (100) = 107.7(1)°	

B amphiboles. The C amphibole occurs as prismatic porphyroblasts up to several centimeters in length and has a bulk composition very similar to those of the Mn-bearing alkali amphilbole described by Roy and Purkait (1968), the magnesio-arfvedsonite–cummingtonite of Robinson et al. (1971), and the Mn-bearing alkali amphibole analyzed by Ghose et al. (1974) (Table 4). Its composition appears to be a complex solid solution of magnesio-riebeckite, magnesio-arfvedsonite, manganese-cummingtonite, and richterite components. On the other hand, the A and B amphiboles have compositions very similar to those of magnesio-arfvedsonite and richterite-rich manganese-cummingtonite, respectively.

Figure 8 shows the idealized M4 site occupancy of the A, B, and bulk C amphiboles and the exsolution lamellae in the C amphibole, plotted on ternary diagrams. The principal variations in M4 occupancy among these amphiboles are in the amounts of Na relative to Mn. The exsolved lamellae and host in "$\bar{1}01$" orientation within the C amphibole have compositions approaching those of the B and A amphiboles, respectively.

Compositions of a bulk sample of the magnesio-arfvedsonite–cummingtonite and the exsolved amphibole pair magnesio-arfvedsonite and manganese-cummingtonite that were reported by Robinson et al. (1971) are also plotted in Figure 8 for comparison. The latter two amphiboles are somewhat similar in composition to the A and B amphiboles in sample SKD of the present study, except that there are significant differences in the Fe^{3+}/Fe^{2+} ratios and in the A-site occupancies, with respect to the amounts of Na and K (see Tables 2, 4). The bulk composition of the magnesio-arfvedsonite–cummingtonite of Robinson et al. (1971) has nearly all Fe as Fe^{3+}. The EMP analyses of C amphibole in the present study have Fe^{3+}/Fe^{2+} ratios similar to that of the magnesio-arfvedsonite–cummingtonite of Robinson et al. but have much higher Fe^{3+}/Fe^{2+} ratios than those of the AEM analyses of the C amphibole. Other studies have shown that some samples of Mn-bearing alkali amphibole contain only Fe^{3+} (Ghose et al., 1986). The oxidized state of Mn^{4+} in associated minerals such as hollandite implies that most Fe must be Fe^{3+}. These relations collectively imply that the ratio of the normalized AEM analyses (Ta-

TABLE 4. Chemical composition of Mn-bearing alkali amphiboles from different localities

Oxides (wt%)	1.	2.	3.	4.	5.	6a.	6b.
SiO_2	55.82	55.78	55.6	54.54	55.32	54.9	55.8
Al_2O_3	0.84	0.59	1.2	1.50	0.10	0.1	0.1
TiO_2	0.19	0.26	0.0	0.75	0.00	n.d.	n.d.
Fe_2O_3	2.16*	6.77*	4.6*	8.93	6.86	8.3**	2.3**
FeO	4.01*	0.67*	2.1*	0.00	<0.50	0.0**	0.0**
MgO	19.72	18.03	17.3	17.11	18.18	17.6	20.8
MnO	7.13	8.70	6.1	7.77	7.65	6.0	15.3
CaO	2.54	2.09	3.1	3.11	2.11	2.3	0.7
Na_2O	5.00	3.99	5.3	4.84	4.65	5.7	1.1
K_2O	0.47	0.24	1.4	1.08	1.97	2.2	0.1
F	n.d.	0.75	n.d.	n.d.	0.15	n.d.	n.d.
H_2O^+	2.12†	1.74†	2.1†	0.38	2.98	2.1†	2.1†
$-(O = F)$	n.d.	−0.16	n.d.	n.d.	−0.03	n.d.	n.d.
TOTAL	100.00‡	99.46	98.8	100.01	99.94	99.2	98.3
Si	7.90	7.99	7.96	7.66	7.94	7.89	8.01
[4]Al	0.10	0.01	0.04	0.25	0.02	0.02	0.00
TOTAL T site	8.00	8.00	8.00	7.91	7.96	7.91	8.01
[6]Al	0.04	0.09	0.16	0.00	0.00	0.00	0.02
Ti	0.02	0.03	0.00	0.08	0.00	n.d.	n.d.
Fe^{3+}	0.23	0.73	0.50	0.94	0.74	0.90	0.25
Mg	4.16	3.86	3.69	3.58	3.88	3.77	4.45
Fe^{2+}	0.47	0.08	0.25	0.00	0.00	0.00	0.00
Mn	0.08	0.21	0.40	0.40	0.38	0.33	0.28
TOTAL M1–M3	5.00	5.00	5.00	5.00	5.00	5.00	5.00
Mn	0.78	0.84	0.35	0.52	0.55	0.41	1.58
Ca	0.38	0.32	0.47	0.47	0.32	0.35	0.11
Na	0.84	0.84	1.18	1.01	1.13	1.24	0.31
TOTAL M4 site	2.00	2.00	2.00	2.00	2.00	2.00	2.00
Na	0.54	0.27	0.29	0.31	0.16	0.35	0.00
K	0.08	0.04	0.25	0.19	0.36	0.40	0.02
TOTAL A site	0.62	0.31	0.54	0.50	0.52	0.75	0.02
F	n.d.	0.34	n.d.	n.d.	0.07	n.d.	n.d.
OH	2.00†	1.66†	2.00†	0.35	2.86	2.00†	2.00†

Note: 1. = Average AEM analysis of the C amphibole from samples SKD and SR2 in the present study; 2. = Average EMP analysis of the C amphibole, sample SKD; 3. = EMP analysis of the sample from Tirodi, Madhya Pradesh, India (Ghose et al. 1974); 4. = Sample from Gowari Wadhona, Madhya Pradesh, India (Roy and Purkait, 1968); 5. = Magnesio-arfvedsonite–cummingtonite from Labrador, Canada; 6a. and 6b. = EMP analyses of the exsolved pair magnesio-arfvedsonite and manganese-cummingtonite, respectively, in the magnesio-arfvedsonite–cummingtonite (Robinson et al., 1971); Analyses 4. and 5. are wet-chemical analyses; n.d. = not determined.
* Fe^{2+} and Fe^{3+} calculated on the basis of normalized structural formula and charge balance.
** Total Fe calculated as Fe^{3+}.
† Calculated assuming 2(OH,F) per structural formula.
‡ Assuming oxides + H_2O^+ = 100.00 wt%.

bles 1, 2) are too small but are reported as such, as other nomenclature schemes are unsatisfactory.

In order to show relations between the M4 occupancy and the amounts of Fe^{3+} of these amphiboles, a plot is given for Na in the M4 site with respect to R^{3+} in the octahedral site (mainly in the M2 site) in Figure 9. The major compositional differences in the amphiboles in the present study are in the amounts of R^{3+} in the M2 site and the amounts of Na (vs. Mn) in the M4 site. The A amphibole and one of the unmixed phases of each set of lamellae in the C amphibole contain high concentrations of Fe^{3+} and Na. These Na-Fe^{3+}-rich amphiboles also contain less Mg in the M2, M1, or M3 sites and less Mn in the M4 site than the Mn-Mg-rich amphiboles. This cation exchange can be ideally expressed as $^{[M4]}Na^+ + {}^{[M2]}Fe^{3+} \leftrightarrow {}^{[M4]}Mn^{2+} + {}^{[M2]}Mg^{2+}$.

Based on the coexisting amphibole pairs (A and B) and the exsolution texture developed only in the C amphibole with intermediate composition, it appears that there is a miscibility gap between the A amphibole and the B amphibole, these two phases corresponding to a Mn-bearing alkali amphibole and manganese-cummingtonite with some richterite component, respectively. The miscibility gap is caused principally by differences in radii of the cations in the M4 (Na vs. Mn) and M2 (Fe^{3+} vs. Mg) sites, as discussed above. Miscibility gaps have been previously reported for alkali amphiboles and ferromagnesian amphiboles as represented by the pair magnesio-arfvedsonite and manganese-cummingtonite, both containing exsolution lamellae, in samples from a metamorphosed Fe formation from Labrador, Canada (Klein, 1966, 1968; Robinson et al., 1971), and by exsolution lamellae of cummingtonite in glaucophane from eclogite assemblages in northern Vermont (Smelik and Veblen, 1991). In addition, coexisting pairs of alkali and ferromagnesian amphiboles, although without exsolution-derived textures, are consistent with the presence of a miscibility gap (Black, 1973; Kimball and Spear, 1984; Evans, 1986).

The term "tirodite," if consistent with the original terminology used by Dunn and Roy (1938), was applied to Mn-bearing amphiboles with bulk compositions includ-

Fig. 9. Plot of Na vs. R^{3+} for the Mn-bearing alkali amphiboles, including C amphibole (C), exsolved "$\overline{1}01$" ($\overline{1}01$A: host, $\overline{1}01$B: lamellae) and "100" lamellae (100A: host, 100B: lamellae), and A amphibole (A) from sample SR2, and B amphibole (B) from sample SKD.
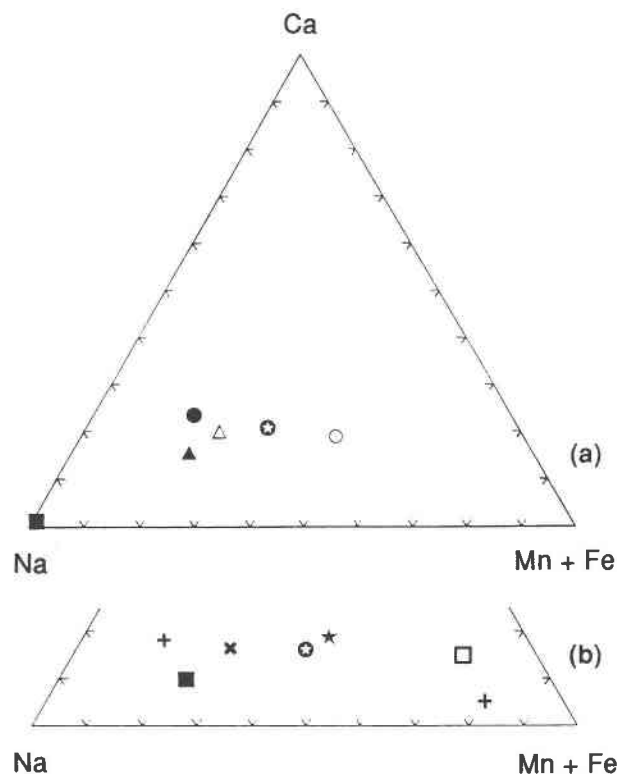
Fig. 8. Ternary diagrams showing idealized M4 site occupancy for the C amphibole (bulk compositions, circled star and closed star), A amphibole inclusions (closed square), B amphibole inclusions (open square), exsolution lamellae and host in "$\overline{1}01$" orientation (open and closed circles) and "100" orientation (open and closed triangles) in the C amphibole. (a): sample SR2, (b): sample SKD; star = average EMP analyses, all others are average AEM analyses. The pair magnesio-arfvedsonite and manganese-cummingtonite (+) and bulk sample (×) reported by Robinson et al. (1971) are plotted in **b** for comparison.

ing (Mn-bearing) alkali amphibole, manganese-cummingtonite with some richterite component, and lesser sodic-calcic amphibole components. However, because of the presence of a miscibility gap between alkali amphibole and ferromagnesian amphibole at relatively low temperatures, this "tirodite" is expected to contain submicroscopic exsolution textures, as observed in the present study (also in Ghose et al., 1974 and Phakey and Ghose, 1974). Its bulk composition is somewhat similar to that of magnesio-arfvedsonite–cummingtonite from Labrador, Canada, which has exsolved into two microscopically distinguishable phases, magnesio-arfvedsonite and manganese-cummingtonite (Klein, 1966, 1968; Robinson et al., 1971; see Table 4, Fig. 8). The bulk sample of the magnesio-arfvedsonite–cummingtonite is apparently another example of "tirodite." Therefore, the term "tirodite" used in the old terminology (e.g., Dunn and Roy, 1938) is not representative of a single amphibole species.
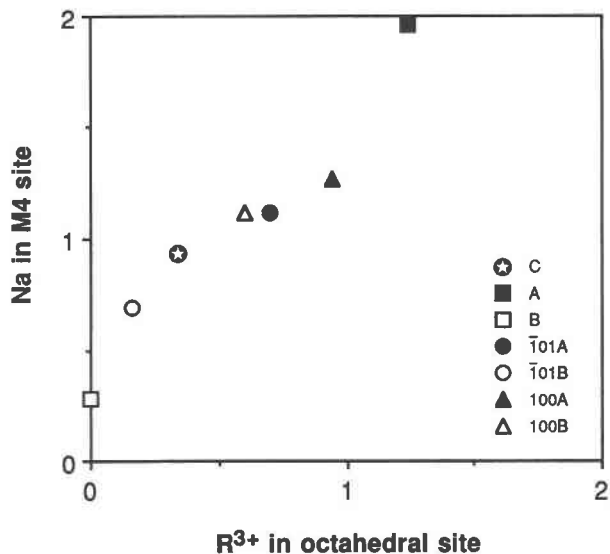
Orientation of the exsolution lamellae

Exsolution lamellae in clinoamphiboles commonly occur with orientations nearly parallel to ($\overline{1}01$) and (100) (see reviews by Ghose, 1981, and Robinson et al., 1982). However, Smelik and Veblen (1991) have reported an exception in which exsolution lamellae of cummingtonite are oriented nearly parallel to ($28\overline{1}$) and ($2\overline{8}\overline{1}$) of glaucophane. Smelik et al. (1991) also reported exsolution lamellae in actinolite + hornblende assemblages nearly parallel to ($13\overline{2}$) and ($1\overline{3}\overline{2}$). The orientations of exsolution lamellae are determined by dimensional misfit between their lattices (e.g., Bollman and Nissen, 1968; Robinson et al., 1971; Fleet, 1982). The common "$\overline{1}01$" and "100" lamellae occur in amphiboles where the two lattices have identical b parameters (Robinson et al., 1971, 1977). The orientations of cummingtonite lamellae near ($28\overline{1}$) and ($2\overline{8}\overline{1}$) in glaucophane, on the other hand, occur in amphiboles that have significantly different b parameters (Smelik and Veblen, 1991).

The orientations of exsolution lamellae in the Mn-bearing alkali amphibole (the C amphibole) were determined using [010] zone SAED patterns and TEM images in which the interfaces between the lamellae and host are sharp for the "$\overline{1}01$" lamellae (Fig. 4). The interfaces of "100" lamellae are diffuse for all viewing directions. The "$\overline{1}01$" lamellar interfaces deviate from ($\overline{1}01$) planes of the Na-Fe^{3+}-rich amphibole by 11.3°. They are very nearly parallel to ($\overline{1}0,0,7$). The interfaces of "100" lamellae deviate from (100) planes by 4.5° and are very nearly parallel to ($24,0,\overline{1}$). The principal differences in lattice parameters for the two sets of "$\overline{1}01$" lamellae are in a ($\Delta a = 0.13$ Å) and β ($\Delta\beta = 1.5°$) (Table 3). The deviations

in orientation for "$\bar{1}01$" and "100" lamellae from ($\bar{1}01$) and (100), respectively, are simlar to those of the exsolution lamellae of magnesio-arfvedsonite and manganese-cummingtonite from Labrador Fe formations, and are consistent with the optimal phase boundary theory (cf. Robinson et al., 1971).

Mechanisms of exsolution and intergrowth formation

Lattice-fringe images (Fig. 6) show that (110) lattice fringes are continuous across the interfaces of "$\bar{1}01$" lamellae. Because of differences in a and β, d_{110} for the Na-Fe^{3+}-rich phase (host) is slightly larger than that of the Mn-Mg-rich phase (lamellae). Continuity in (110) fringes can therefore occur without fringe terminations occurring periodically along the interface (i.e., without becoming semicoherent) if the fringes change angle across the interface. Coherence across the two-amphibole interface, with a minimum strain energy, is therefore maintained by a slight change (of about 1.5°) of the (110) orientation across the "$\bar{1}01$" interface.

The two sets of streaks associated with reflections in the SAED patterns are perpendicular to the "$\bar{1}01$" and "100" lamellae in real space, respectively. The cause of the streaks perpendicular to "$\bar{1}01$" is probably different from that of the streaks perpendicular to "100". Because the interfaces of "$\bar{1}01$" lamellae are sharp (Figs. 4, 5), continuous modulation of composition or lattice parameters can be excluded. For a coherent interface, the matching of the two lattices creates elastic strain within the coherent lattice planes (the lattice planes perpendicular or nearly perpendicular to the interface) and also within all other lattice planes, including those parallel to the lamellar interface (cf. Yund and Tullis, 1983). The streaks perpendicular to "$\bar{1}01$" therefore appear to be caused by continuous change in the spacing of the lattice planes that are approximately parallel to the lamellar interfaces, with increasing distance from the interface. Similar streaks connecting the discrete reflections from augite and pigeonite lamellae have also been observed and interpreted as caused by coherency across lamellar interfaces (e.g., Grove, 1982). On the other hand, the streaks perpendicular to "100" lamellae are probably caused by continuous modulation of composition and lattice parameters because the "100" lamellae are generally very fine and show vague boundaries and nondistinctive contrast even with edge-on orientations. The abundant "$\bar{1}01$" and "100" lamellae are generally homogeneously distributed in the C amphibole. Therefore, the "$\bar{1}01$" lamellae might have formed by homogeneous nucleation and growth or by spinodal decomposition and further growth into discrete phases. The "100" lamellae display a small width and a diffuse interface, as consistent with spinodal decomposition (Fig. 4). These criteria have been used as indicative of spinodal decomposition of augite-pigeonite (Champness and Lorimer, 1976) and actinolite-hornblende (Smelik et al., 1991). However, the "100" lamellae in some samples show widths and split reflections similar to those of the "$\bar{1}01$" lamellae (Fig. 7). They appear to have grown as discrete phases and were not necessarily exsolved by spinodal decomposition.

Coexistence of the A amphibole and the B amphibole as small inclusions within the C amphibole clearly implies nonequilibrium conditions. The A and B amphiboles are near magnesio-arfvedsonite and manganese-cummingtonite in composition, respectively, but the C amphibole has an intermediate composition and has unmixed to form amhiboles with compositions approaching those of the A and B amphiboles. These relations imply that the A and B amphiboles and exsolution lamellae all formed under retrograde metamorphic conditions following formation of a single homogeneous C amphibole at peak metamorphic conditions. During cooling, the "$\bar{1}01$" and "100" lamellae formed in the C amphibole through spinodal decomposition or homogeneous nucleation and growth. The "$\bar{1}01$" lamellae generally have greater widths than those of the "100" lamellae, although both may have similar widths, as shown in Figure 7. This is similar to the exsolution in augite-pigeonite pairs, in which "001" lamellae generally have a greater width than that of "100" lamellae (e.g., Champness and Lorimer, 1976). The micrometer-sized grains of A and B amphiboles most likely have formed through a fluid-mediated dissolution and recrystallization process that affected only limited domains, either of the original unexsolved C amphibole or of amphibole that had already been subject to exsolution. Such nonpervasive alteration may have occurred under closed-system conditions, as amphibole compositions are retained where cracks or other imperfections led to the access of fluids.

REFERENCES

Black, P.M. (1973) Mineralogy of New Caledonian metamorphic rocks. II. Amphiboles from Ouégoa District. Contributions to Mineralogy and Petrology, 39, 55–64.
Bollman, W., and Nissen, H.-U. (1968) A study of optimal phase boundaries: The case of exsolved feldspars. Acta Crystallographica, 24A, 546–557.
Champness, P.E., and Lorimer, G.W. (1976) Exsolution in silicates. In H.-R. Wenk, J.M. Christie, J.M. Cowley, A.H. Heuer, G. Thomas, and N.J. Tighe, Eds., Electron microscopy in mineralogy, p. 174–204. Springer-Verlag, New York.
Cliff, G., and Lorimer, G.W. (1975) The quantitative analysis of thin specimens. Journal of Microscopy, 103, 203–207.
Dunn, J.A., and Roy, P.C. (1938) Tirodite, a manganese amphibole from Tirodi, Central Provinces. Record, Geological Survey of India, 73, 295–298.
Evans, B.W. (1986) Reactions among sodic, calcic, and ferromagnesian amphiboles, sodic pyroxene, and deerite in high-pressure metamor-

phosed ironstone, Siphnos, Greece. American Mineralogist, 71, 1118–1125.

Fleet, M.E. (1982) Orientation of phase and domain boundaries in crystalline solids. American Mineralogist, 67, 926–936.

Ghose, S. (1981) Subsolidus reactions and microstructures in amphiboles. In Mineralogical Society of America Reviews in Mineralogy, 9A, 325–372.

Ghose, S., Forbes, W.C., and Phakey, P.P. (1974) Unmixing of an alkali amphibole (tirodite) into magnesio-richterite and magnesio-riebeckite. Indian Journal of Earth Sciences, 1, 37–42.

Ghose, S., Kershen, M., Langer, K., Rossi, G., and Ungaretti, L. (1986) Crystal field spectra and Jahn-Teller effect of Mn^{3+} ions in clinopyroxene and clinoamphiboles from India. Physics and Chemistry of Minerals, 3, 291–305.

Grove, T.L. (1982) Use of exsolution lamellae in lunar clinopyroxenes as cooling rate speedometers: An experimental calibration. American Mineralogist, 67, 251–268.

Kimball, K.L., and Spear, F.S. (1984) Metamorphic petrology of the Jackson County Iron Formation, Wisconsin. Canadian Mineralogist, 22, 605–619.

Klein, C., Jr. (1966) Mineralogy and petrology of the metamorphosed Wabush iron formation, Southwestern Labrador. Journal of Petrology, 7, 246–305.

——— (1968) Coexisting amphiboles. Journal of Petrology, 9, 281–330.

Leake, B.E. (1978) Nomenclature of amphiboles. American Mineralogist, 63, 1023–1053.

Phakey, P.P., and Ghose, S. (1974) Study of unmixing of an alkali amphibole. Diffraction studies of real atoms and real crystals. Australian Academie of Sciences, 11, E-2, 171–172.

Robinson, P., Jaffe, H.W., Ross, M., and Klein, C., Jr. (1971) Orientation of exsolution lamellae in clinopyroxenes and clinoamphiboles: Consideration of optimal phase boundaries. American Mineralogist, 56, 909–939.

Robinson, P., Ross, M., Nord, G.L., Jr., Smyth, J.R., and Jaffe, H.W. (1977) Exsolution lamellae in augite and pigeonite: Fossil indicators of lattice parameters at high temperature and pressure. American Mineralogist, 62, 857–873.

Robinson, P., Spear, F.S., Laird, J., Klein, C., Evans, B.W., and Doolan, B.L. (1982) Phase relations of metamorphic amphiboles: Natural occurrence and theory. In Mineralogical Society of America Reviews in Mineralogy, 9B, 1–227.

Roy, S. (1966) Syngenetic manganese formations of India, 219 p. Jadavpur University Press, Calcutta.

Roy, S., and Purkait, P.K. (1968) Mineralogy and genesis of metamorphosed manganese silicate rocks (gondite) of Gowari Wadhona, Madhya Pradesh, India. Contributions to Mineralogy and Petrology, 20, 86–114.

Shau, Y.-H., Peacor, D.R., Ghose, S., and Phakey, P.P. (1989) Transmission electron microscopic study of spinodal decomposition in Mn-bearing alkali amphibole ("tirodite") from India (abs.). Eos, 70, 353.

Shau, Y.-H., Peacor, D.R., and Essene, E.J. (1990) Corrensite and mixed-layer chlorite/corrensite in metabasalt from northern Taiwan: TEM/AEM, EMPA, XRD, and optical studies. Contributions to Mineralogy and Petrology, 105, 123–142.

Shau, Y.-H., Feather, M.E., Essene, E.J., and Peacor, D.R. (1991) Genesis and solvus relations of submicroscopically intergrown paragonite and phengite in a blueschist from Northern California. Contributions to Mineralogy and Petrology, 106, 367–378.

Smelik, E.A., and Veblen, D.R. (1989) A five-amphibole assemblage from blueschist in northern Vermont, American Mineralogist, 74, 960–965.

——— (1991) Exsolution of cummingtonite from glaucophane: A new orientation for exsolution lamellae in clinoamphiboles. American Mineralogist, 76, 971–984.

Smelik, E.A., Nyman, M.W., and Veblen, D.R. (1991) Pervasive exsolution within the calcic amphibole series: TEM evidence for a miscibility gap between actinolite and hornblende in natural samples. American Mineralogist, 76, 1184–1204.

Spear, F.S. (1982) Phase equilibria of amphiboles from the Post Pond Volcanics, Mt. Cube Quadrangle, Vermont. Journal of Petrology, 23, 383–426.

Yund, R.A., and Tullis, J. (1983) Subsolidus phase relations in the alkali feldspars with emphasis on coherent phases. In Mineralogical Society of America Reviews in Mineralogy, 2, 141–176.